

# Timing Resolution Performance Comparison for Fast and Standard Outputs of SensL SiPM

Sergei Dolinsky, Geng Fu, and Adrian Ivan

**Abstract**– A new silicon photomultiplier (SiPM) with a unique fast output signal feature was recently introduced by SensL. For a SiPM device with  $3 \times 3 \text{ mm}^2$  sensitive area, the single photo electron response from the fast output is less than 2 ns wide compared with 50 ns width observed at the standard output. Using the fast readout signal, a coincidence resolving time (CRT) of 190 ps (FWHM - full width at half maximum) was measured with a  $3 \times 3 \times 10 \text{ mm}^3$  LYSO crystal optically coupled to the SiPM mounted on the SensL MicroFB-SMA evaluation board. Applying additional C-R high pass filters to the standard SiPM output, we shortened the SPE response from 50 ns to 3 ns width and measured CRT values similar to those obtained with fast output signals. We have studied the effect of external filtering on CRT with two SensL  $3 \times 3 \text{ mm}^2$  devices with different microcell sizes (35  $\mu\text{m}$  and 50  $\mu\text{m}$ ). For both devices studied, we demonstrated similar CRT performance between the fast output and standard output with optimized pulse shaping filter. However, for applications requiring simultaneous measurement of intensity and timing of light pulses, the availability of a separate fast output directly from the sensor is convenient because it reduces the need for additional circuits and provides CRT performance equal to external filters optimized for the standard outputs.

## I. INTRODUCTION

TIMING performance is important for many applications of scintillator detectors, such as TOF-PET (Time of Flight Positron Emission Tomography) [1,2], gamma-ray astrophysics [3], or high energy physics experiments. Silicon photomultipliers have evolved from the well-known single photon avalanche diodes (SPAD) [4] operating with high multiplication gain in Geiger avalanche mode but limited to active areas of the order ( $\sim$ ) of  $10^{-2} \text{ mm}^2$ . Recently, SiPMs with sensitive areas  $\sim 10 \text{ mm}^2$  per pixel became commercially available from multiple vendors and have shown steady improvement in performance [5] (e.g., lower noise level, better photon detection efficiency at shorter wavelengths, and better timing resolution.)

In contrast with the widely used vacuum photomultiplier tubes (PMT), SiPMs present a compact form factor and immunity to magnetic fields and mechanical stress, which resulted in their rapid adoption in applications where such properties are required, such as in medical scanners with simultaneous TOF-PET and MR imaging capability [6]. From the point of view of TOF-PET performance, a comparison between SiPMs and PMTs should consider the critical

parameters contributing to the signal/noise ratio (SNR) and detector coincidence resolving time. The photon detection efficiency (PDE), the photoelectron multiplication gain, and the intrinsic dark count rate (DCR) determine effectively the SNR, while the shape of the single photo-electron (SPE) response has an additional influence on CRT. The above parameters are compared for reference in Table I, based on data available from vendors of fast PMTs and SiPM devices. It is noticeable that SiPMs can now equal or surpass the signal level of PMTs but their noise and pulse shape can still be improved for high performance timing applications.

TABLE I. COMPARISON OF TYPICAL PMT AND SIPM PARAMETERS RELEVANT FOR TIMING APPLICATIONS WITH SCINTILLATOR-BASED DETECTORS

Parameter	PMT	SiPM
Photon detection efficiency (PDE)	25% (bi-alkali) ( $\sim 40\%$ UBA)	40-60%
Photoelectron multiplication gain (M)	$\sim 10^6$	$\sim 10^6$
Dark counts rate (DCR) [ $\text{kHz}/\text{mm}^2$ ]	0.01-0.1	100-1000
Single photo electron (SPE) response:		
-Rise time	0.7 ns	1 ns
-Full width at half maximum (FWHM)	1.2 ns	20-50 ns

Decreasing DCR has been a permanent goal over the last years for SiPM manufacturers. Successful DCR reduction has been made possible through silicon material selection and improved SiPM fabrication processes [5].

## II. OVERVIEW OF SIPM TIMING PERFORMANCE

Compared to fast PMTs, standard SiPMs present particularly longer tails in their SPE pulse shape due to the mechanism of signal generation by avalanche multiplication and its passive quenching. The Geiger avalanche discharges quickly the capacitance  $C_d$  of the microcells below breakdown voltage and quenches the multiplication process. The microcells recharge slowly with current limited by the quench resistance  $R_q$ . The standard output of SiPM is the recharging current which has an exponential time constant ( $\tau_{\text{SPE}}$ ) determined by [7]:

$$\tau_{\text{SPE}} = C_d \cdot (R_q + R_{\text{Input}} \cdot N_{\text{microcells}}) \quad (1)$$

Typical values of  $R_q$  and  $C_d$  explain the long SPE pulse tails observed in standard SiPMs. Fig.1 illustrates this important difference between PMT and SiPM with (a) SPE pulse shapes and (b) scintillator waveforms.

For TOF-PET applications, one of the most important performance parameters affecting CRT is the rise time of the signal produced by the scintillation light created by annihilation photons. Fig.1b shows the difference in pulse shapes of LYSO scintillations detected by the fast PMT and the SiPM, respectively.

Manuscript received November 21, 2013.

S. Dolinsky, G. Fu, and A. Ivan are with the General Electric Global Research Center, Niskayuna, NY, 12309, USA.

Corresponding author: Sergei Dolinsky, General Electric Global Research Center, Niskayuna, NY, 12309, USA (telephone: 518-387-5400, e-mail: dolinsky@research.ge.com).

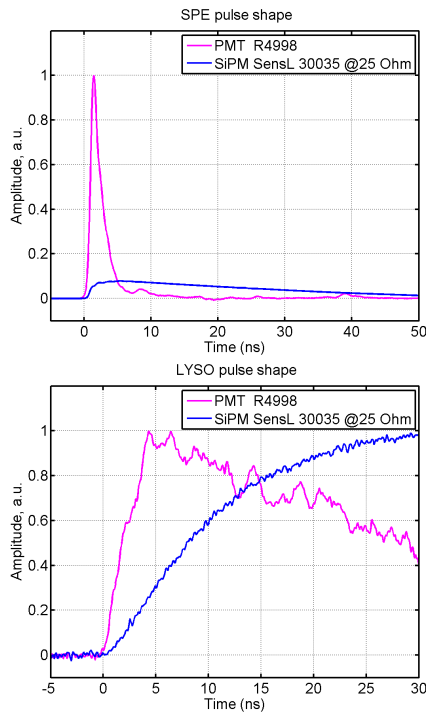


Figure 1: (a) Top: Single photo electron (SPE) pulse shape from the anode of a fast PMT (Hamamatsu R4998) and the standard output of an SiPM (SensL MicroFB-SMA-30035). The signals are normalized such that they have equal total charge; (b) Bottom: Rising edge of the voltage signals from the full 511 keV absorption in LYSO scintillator detected with the fast PMT and SiPM device, respectively, showing the slowdown effect of the long SPE tail. The signals are normalized by their peak value.

The characteristic time  $\tau_{\text{SPE}} = 50$  ns for the SiPM studied (also typical for other standard SiPMs) is much larger than the PMT SPE pulse width of a few nanoseconds. This impacts the scintillation response function, which can be computed as the convolution of the SPE with the time distribution of the scintillation photons arriving at the detector. The long tail of the SiPM SPE effectively reduces the slope  $dV/dt$  of the 511 keV scintillation signal, as observed in Fig. 1b, in contrast with the sharp rise of the PMT response. Since all timing pick-off methods essentially time stamp the scintillation signal at the moment of crossing a predetermined voltage threshold, the time jitter associated with the method is given by:  $\sigma_{\text{time}} = \sigma_V \cdot (dV/dt)^{-1}$ . For equal charge gains in the PMT and SiPM, the latter can be at disadvantage for timing applications due to slower rise time.

A typical implementation for TOF-PET detectors built from commercial SiPM devices consists in feeding the SiPM signal into an amplifier with an input load resistance  $R_{\text{Input}}$ . In order to improve timing, it is desirable that the amplifiers have a low noise and low impedance ( $R_{\text{Input}} \ll R_q/N_{\text{microcells}}$ ) to reduce the SPE fall time  $\tau_{\text{SPE}}$  to the minimum value,  $C_d \cdot R_q$ . This practical solution has been used [6] to build and evaluate the timing performance of new SiPM-based TOF-PET detectors. In parallel, several studies have tried to model SiPM devices and predict the timing resolution of scintillator detectors built with them. To date, this effort has had limited success due to the complex interdependence of SiPM parameters (gain, dark current, crosstalk, and signal propagation delay and jitter) with

the scintillator optical parameters (light yield, rise and decay time, dimensions, and surface finish). Experimental tests remain the best method for evaluating the performance of new improvements to current SiPM technology.

### III. SENS� SiPM WITH FAST OUTPUT

#### A. Concept and Implementation

SensL (Cork, Ireland) has developed a proprietary [8] fast mode output in addition to the standard output available in previous SiPM devices. The conventional SiPM is in essence a parallel array of microcells, with each microcell consisting of an individual p-n junction structure operating as an avalanche diode above breakdown voltage. All microcell diodes are connected in parallel via quench resistors. A photon can trigger a Geiger-mode avalanche which develops very fast ( $<1$  ns), so the observed rise time at the standard output is determined only by stray capacitances and inductances. However, the fall time  $\tau_{\text{SPE}}$  is determined by the quench resistor values and the total capacitance of the microcells, as in eq. (1), and is typically in the range of tens of nanoseconds.

SensL has developed SiPM with a third electrode which is coupled to individual diodes through low capacitance. As a result, the response signal has very short pulse width. According to [8], the capacitance of the third electrode toward the other electrodes of the SiPM is  $\sim 10\%$  of  $C_{\text{SiPM}}$ .

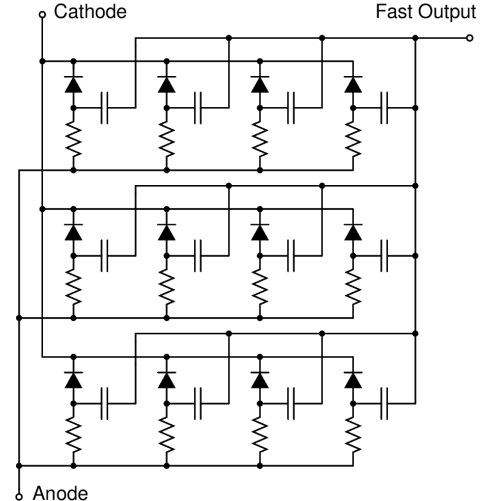


Figure 2: Concept schematic of the SensL fast output SiPM shown as an array of microcells connected in parallel (Courtesy of SensL [9].) Each diode symbol represents an individual p-n junction microstructure. Unlike standard SiPMs, each junction in the SensL device has a connection to a third electrode with a low capacitive coupling.

As shown in the conceptual schematic in Fig.2, the third electrodes are coupled to a common “Fast Output” terminal. Because the equivalent capacitance is reduced by an order of magnitude, the signal collected from the fast output has a much shorter fall time than the conventional output signal.

We have used the SensL evaluation board MicroFB-SMA-30035 to study the shape of LYSO scintillation events from the standard output and the fast output connected to a 1 GHz, low-noise amplifier (ZFL-1000H+, Mini-Circuits). The SiPM was optically coupled to a  $3 \times 3 \times 10$  mm<sup>3</sup> Teflon-wrapped LYSO crystal and exposed to a gamma source. The two

amplified output signals were input into a fast oscilloscope (1 GHz Waverunner 610Zi, Teledyne LeCroy) and shown in Fig.3.

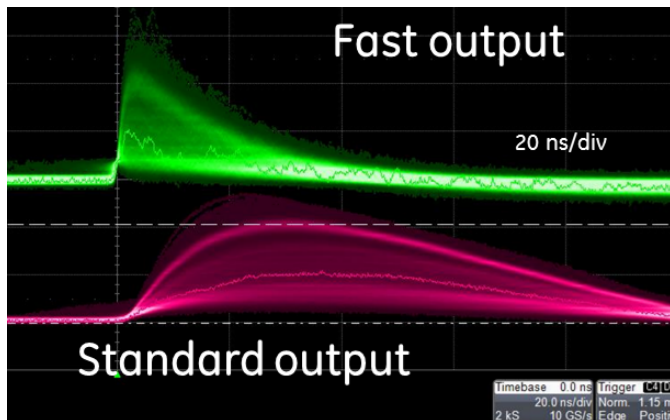


Figure 3: Waveforms from LYSO crystal exposed to a gamma source and optically coupled to the “fast output” SiPM device available on the SensL evaluation board MicroFB-SMA-30035. The fast output signals (green) present a five-fold reduction in pulse fall time compared to the standard output signals (red).

### B. Experimental Evaluation

In order to evaluate the advantage of the fast output over the conventional output for TOF-PET applications, we have used the SensL test board together with the LYSO crystal as described above in coincidence with a reference detector (LaBr<sub>3</sub> crystal on a fast PMT, R4998, Hamamatsu Corp.) A typical fast-slow coincidence setup [10] was implemented using standard NIM and CAMAC electronic modules. The simple block diagram shown in Fig. 4 illustrates the CRT measurement setup. The PMT anode output was split into two signals: E1 for energy measurement and T1 for the timing circuit. The two SensL test board outputs, S\_OUT for standard output and F\_OUT for fast output, were connected differently depending on which output was chosen to form the timing signal T2. When standard output was selected for timing, S\_OUT was connected to the fast amplifier ZFL-1000H+ and F\_OUT connected to a NIM amplifier (PS-775, Phillips Scientific) to form the energy signal E2. In the case when T2 was derived from the fast output, F\_OUT was connected to the ZFL-1000H+ amplifier and S\_OUT was attenuated (inset, Fig.4). In both versions of the setup, the timing signals were presented to a leading edge discriminator (PS-704, Phillips Scientific) which produced a standard fast NIM timing signal. The threshold of the T2 discriminator was varied as described later. The energy signals E1 and E2 and the time difference (T1-T2) were digitized, producing the energy spectra and the time coincidence distribution for each set of measurements.

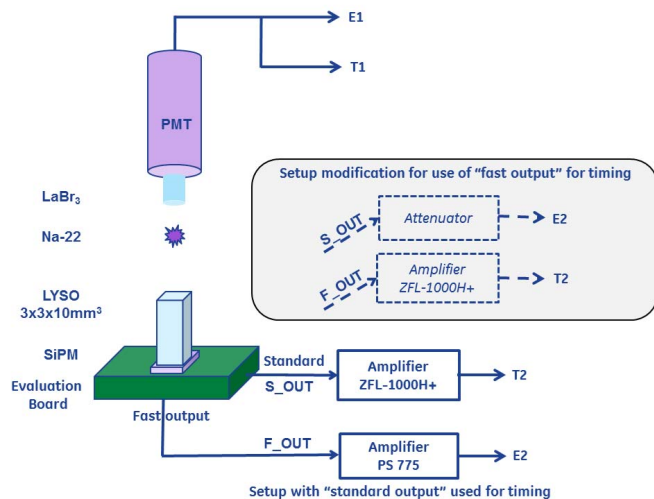


Figure 4: CRT measurement setup with a fast reference detector (LaBr<sub>3</sub> on PMT), a source of 511 keV annihilation photons (<sup>22</sup>Na), and the LYSO crystal coupled to the SensL SiPM on the evaluation board MicroFB-SMA-30035. The inset shows the modification used to generate the timing signal T2 from the fast output F\_OUT, instead of the standard output S\_OUT.

The energy spectra were used to select only the events with full 511 keV energy deposition in both detectors and the timing signals were corrected for pulse amplitude dependence (amplitude walk effect [10]). From the Full Width at Half Maximum (FWHM) of the measured time coincidence distribution we then subtracted in quadrature the known timing resolution of the reference detector and multiplied the result by  $\sqrt{2}$  to represent the estimated CRT of the SiPM detector in coincidence with an identical SiPM detector, as in a PET scanner.

As expected, CRT varied when the bias voltage and the discriminator threshold were changed. Fig. 5a presents the measured CRT dependence on  $V_{bias}$  and  $V_{thresh}$ , when using for timing the standard output of a  $3 \times 3$  mm<sup>2</sup> SensL SiPM with 35  $\mu$ m microcell size. For a fixed discriminator threshold, the CRT performance is dominated at low  $V_{bias}$  by the electronics noise and lower PDE, while at high  $V_{bias}$  the fast increase of the dark counts rate becomes the limiting factor. For each bias sweep curve there is an optimal value of  $V_{bias}$  producing the minimum CRT. For the measurements presented in Fig. 5a with standard output timing, the absolute minimum CRT was approximately 220 ps (FWHM). A similar set of curves was obtained using the fast output signal for timing of the same device with 35  $\mu$ m microcells (Fig.5b) with an absolute minimum of 190 ps (FWHM). Similar improvement in CRT was observed with a  $3 \times 3$  mm<sup>2</sup> SensL SiPM with 50  $\mu$ m microcells: Fig 6a shows the set of CRT vs.  $V_{bias}$  data with standard output used for timing and Fig. 6b the corresponding results for fast output timing. The CRT minimum of 230 ps (FWHM) in the standard case was improved to 190 ps (FWHM) when using the fast output.

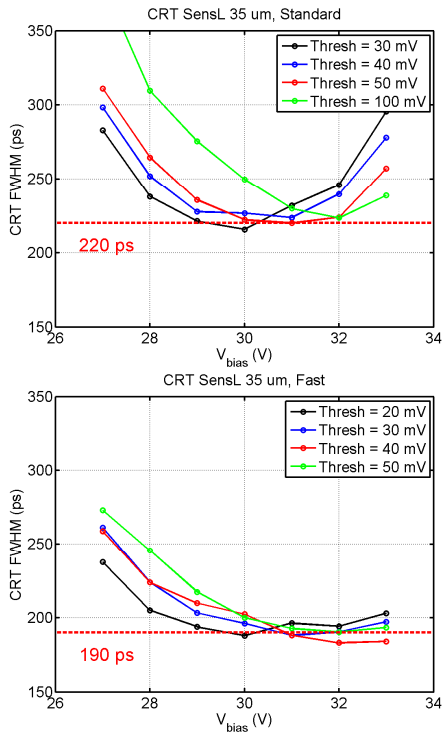


Figure 5: Two sets of measured CRT (FWHM) vs. SiPM bias for a fixed timing comparator threshold (values indicated by legend) for a SensL MicroFB-30035 device ( $3 \times 3$  mm<sup>2</sup> area with 35  $\mu$ m microcells). (a) Top: Standard output signal used for timing. (b) Bottom: Fast output signal used for timing.

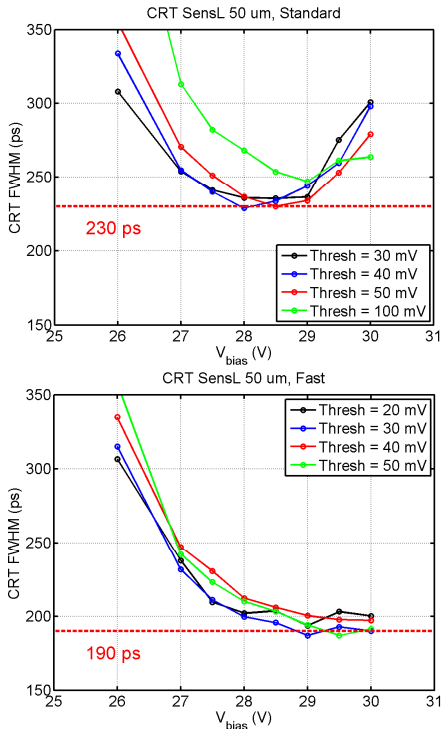


Figure 6: Measured CRT (FWHM) vs. SiPM bias for a fixed timing comparator threshold (values indicated by legend) for a SensL MicroFB-30050 device ( $3 \times 3$  mm<sup>2</sup> area with 50  $\mu$ m microcells). (a) Top: Standard output signal used for timing. (b) Bottom: Fast output signal used for timing.

## IV. EXTERNAL SHAPING

### A. Concept and Simulation

In the case of “standard” SiPMs, a similar improvement in CRT performance could be achieved using an external shaping circuit to decouple the SiPM capacitance and form a faster signal for timing. We have used the SensL devices to test this idea and benchmark the performance from an external shaping applied to the standard output against the performance available with the “fast output” signal.

Before experimenting with external circuits, we used a SPICE model from SensL [9] to simulate the pulse shapes from standard and fast outputs. Fig. 7 shows our model of the SensL SiPM with fast output. The avalanche discharge is simulated as a current source generating a nanosecond impulse in parallel with the capacitance  $C_1$  of the microcell. We have selected the values for microcell quench resistance  $R_1$ , diode capacitance  $C_1$ , and fast coupling capacitance  $C_4$  from forward I-V measurements and SPE gain and pulse shape characterization. The routing and wiring inductances and resistances (parasitic components) were estimated from calculated values of typical traces and are possibly not accurate. From our previous experience with SiPM modeling and measurements, the parasitic components can significantly impact the SPE shape in the beginning of pulse and explain some differences between simulated and measured SPE response in first 1-2 ns, such as overshoot and ringing. Despite the parasitics effects, the SPICE model provided an understanding the pulse shape at the fast output and it was used to test the idea that a similar fast pulse can be produced with an equivalent C-R shaping of the standard output.

### B. Validation

The simulated and measured SPE responses for the three signals (fast, standard, and standard with external C-R shaping) are shown in Fig. 8 and Fig. 9, respectively. Proper external C-R shaping ( $\tau = R \cdot C = 2$  ns) applied to the standard output made the SPE response short and almost identical to the SPE response from the fast output terminal. Fig. 10 illustrates the improved shaping of the LYSO scintillator pulses captured on the oscilloscope from the fast output and the standard output after external 2 ns C-R shaping.

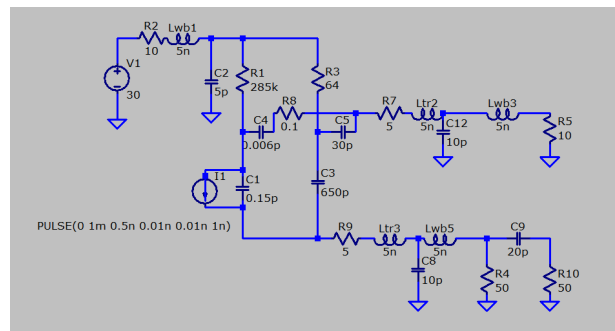


Figure 7: SPICE model circuit for the SensL MicroFB-30035 device ( $3 \times 3$  mm<sup>2</sup> area with 35  $\mu$ m microcells, model courtesy of SensL). Microcell capacitance and resistance values were determined from forward I-V measurements and SPE gain and pulse shape characterization.

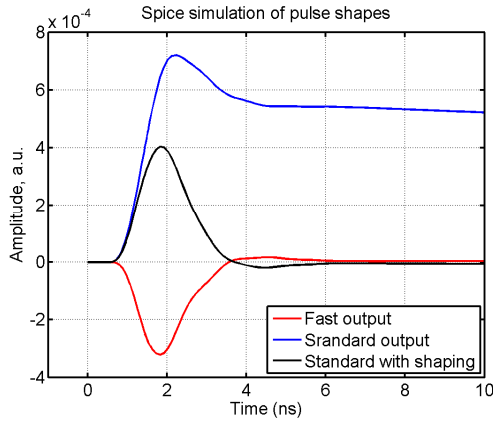


Figure 8: Simulated SPE signals from the SensL MicroFB-30035 device ( $3 \times 3$  mm<sup>2</sup> area with  $35 \mu\text{m}$  microcells): fast output (red), standard output (blue), and (black) standard output connected to an external C-R shaping circuit ( $\tau = 2$  ns).

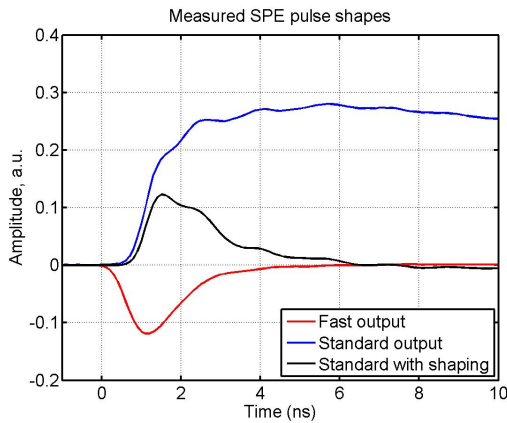


Figure 9: Measured SPE signals from the SensL MicroFB-30035 device ( $3 \times 3$  mm<sup>2</sup> area with  $35 \mu\text{m}$  microcells): fast output (red), standard output (blue), and (black) standard output connected to an external C-R shaping circuit ( $\tau = 2$  ns).

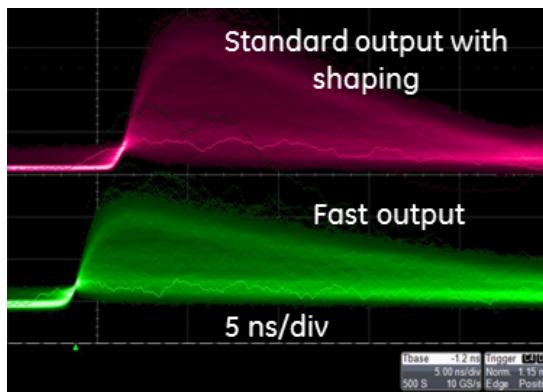


Figure 10: Waveforms from a LYSO crystal exposed to a gamma source and optically coupled to the SensL MicroFB-30035 device ( $3 \times 3$  mm<sup>2</sup> area with  $35 \mu\text{m}$  microcells). The standard output signals with an external 2 ns C-R shaping (red) become similar to the fast output signals (green).

### C. Timing Measurements and Comparison

Using the standard setup from Fig. 4, we have measured the timing performance of the SensL MicroFB-30035 and -30050 devices with a 2 ns C-R shaping circuit connected to the standard output. For the device with  $35 \mu\text{m}$  microcells, the external shaping improved the best CRT from 220 ps (standard output, Fig. 5a) to 180 ps (C-R shaped standard output, Fig. 11). Similarly, the lowest CRT value for the  $50 \mu\text{m}$  device improved from 230 ps (standard, Fig. 6a) to 180 ps (C-R shaped standard output, Fig. 12).

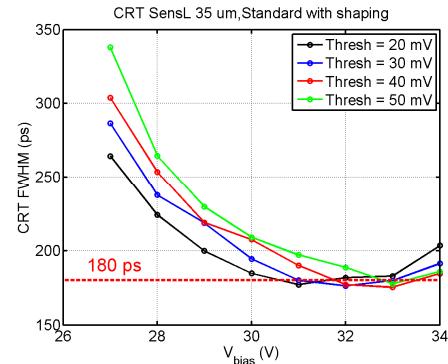


Figure 11: Measured CRT (FWHM) vs. SiPM bias for the SensL MicroFB-30035 device ( $3 \times 3$  mm<sup>2</sup> area with  $35 \mu\text{m}$  microcells) with external C-R shaping ( $\tau = 2$  ns) applied to standard output.

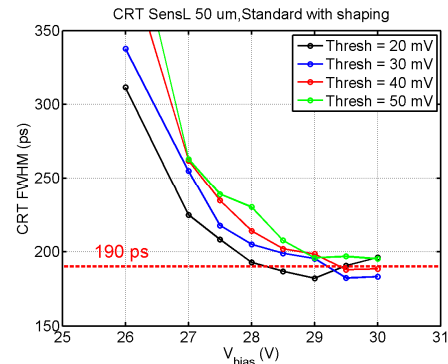


Figure 12: Measured CRT (FWHM) vs. SiPM bias for the SensL MicroFB-30050 device ( $3 \times 3$  mm<sup>2</sup> area with  $50 \mu\text{m}$  microcells) with external C-R shaping ( $\tau = 2$  ns) applied to standard output.

### V. CONCLUSIONS

For both devices studied, we have demonstrated equivalent CRT performance between: (1) the fast output available and (2) the standard output connected to an external shaping filter optimized to match the fast pulse shapes before the timing comparator. For applications requiring simultaneous measurement of intensity and timing of fast light pulses, such as TOF-PET, the availability of a separate fast output directly from the SiPM sensor is convenient because it reduces the need for designing and implementing an additional circuit and provides CRT performance equal to filters optimized for the standard outputs.

## REFERENCES

- [1] M. Conti, "Improving time resolution in time-of-flight PET," *Nucl. Instr. Meth. Phys. Res., Section A*, Vol. 648, Issue SUPPL.1, pp. S194-S198, 2011.
- [2] J. Y. Yeom, R. Vinke, and C. S. Levin, "Optimizing timing performance of silicon photomultiplier-based scintillation detectors," *Physics in Medicine and Biology*, Volume 58, Issue 4, pp. 1207-1220, 2013.
- [3] A. Ulyanov, L. Hanlon, S. McBreen, S. Foley, and D. Byrne, "Study of silicon photomultipliers for the readout of scintillator crystals in the proposed GRIPS Gamma-Ray Astronomy mission," *Proceedings of science*, 9th INTEGRAL Workshop and Celebration of the 10th Anniversary of the Launch, INTEGRAL 2012; Bibliotheque Nationale de France; France; October 15-19, 2012.
- [4] A. Spinelli and A.L. Lacaita, "Physics and numerical simulation of single photon avalanche diodes," *IEEE Transactions on Electron Devices*, Vol. 44, Issue 11, pp. 1931-1943, 1997.
- [5] T. Nagano, K. Sato, A. Ishida, T. Baba, R. Tsuchiya, and K. Yamamoto, "Timing resolution improvement of MPPC for TOF-PET Imaging," in *Conference Record of the 2012 IEEE Nuclear Science Symposium and Medical Imaging Conference*, pp. 1577-1580.
- [6] C.L. Kim, D. McDaniel, J. Malaney, G. McBroom, W. Peterson, V.H. Tran, J. Guo, A. Ivan, S. Dolinsky, A. Wagadarikar, A. Byun, G. Fu, and A. Ganin, "Time-of-Flight PET-MR detector development with silicon photomultiplier," in *Conference Record of the 2012 IEEE Nuclear Science Symposium and Medical Imaging Conference*, pp. 3533-3536.
- [7] S. Dolinsky and S. Zelakiewicz, "Multiplexing requirements for solid state photomultipliers in time-of-flight PET," in *Conference Record of the 2010 IEEE Nuclear Science Symposium and Medical Imaging Conference*, pp. 1763-1766.
- [8] N. Pavlov, "Silicon Photomultiplier and Readout Method", *USPTO Patent Application Publication*, No. US2013/0099100 A1, 2013.
- [9] SensL, private communication.
- [10] G.F. Knoll, *Radiation Detection and Measurement*, 4<sup>th</sup> ed., Wiley: New York, 2010.